Radiative transfer for a three-dimensional raining cloud

J. L. Haferman, W. F. Krajewski, T. F. Smith, and A. Sánchez A.

Satellite-sensor-based microwave brightness temperatures for a three-dimensional raining cloud over a reflecting surface are computed by using a radiative transfer model based on the discrete-ordinates solution procedure. The three-dimensional model applied to a plane layer is validated by comparison with results from a one-dimensional model that is available in the literature. Results examining the effects of cloud height, rainfall rate, surface reflectance, rainfall footprint area, and satellite viewing position on one- and three-dimensional brightness temperature calculations are reported. The numerical experiments indicate that, under certain conditions, three-dimensional effects are significant in the analysis of satellite-sensor-based rainfall retrieval algorithms. The results point to the need to consider carefully three-dimensional effects as well as surface reflectance effects when interpreting satellite-measured radiation data.

Key words: Radiative transfer, clouds, rain, brightness temperature, discrete-ordinates method.

Introduction

The spatial distribution of rainfall around the Earth is indicative of energy transport patterns in the atmosphere and has important implications for global climatic modeling.[1] Quantitative observations of rainfall over open ocean provide a direct estimation of the amount of latent heat released to the atmosphere, which is a significant component of the atmospheric energy budget. For obvious reasons, satellites offer the only viable means of estimating global oceanic rainfall. Satellite-based methods of rainfall estimation, however, are indirect in that the satellite sensors measure radiation energy and not rainfall. The measured radiation energy is the result of many processes, not only rainfall. For example, in the visible band of the spectrum, a sensor detects clouds but not necessarily the rain produced by the clouds.

The inversion of satellite-measured radiation to rainfall rates can be accomplished in many ways that are reviewed by Arkin and Ardanuy.[2] At the present time, the most promising approach to oceanic rainfall estimation is through the use of microwave observations from the Defense Meteorological Satellite Program (DMSP) polar-orbiting satellite. In the microwave part of the spectrum, the ocean looks cold and provides a good background for the warm-looking rainfall. Several researchers have demonstrated the usefulness of the microwave channel in a quantitative estimation of rainfall.[3–6] To better understand the uncertainties in the interpretation of microwave observations, it is necessary to develop simulation tools that can account for small-scale variability of rainfall and the associated processes of emission and scattering that are due to rain and cloud liquid water and ice droplets. At microwave frequencies, the footprint of the DMSP satellite is rather large (69 × 40 km at 19.35 GHz): therefore, the subpixel variability is an important component of the overall error in the rainfall estimation. Proper analysis of these effects can be achieved by using a three-dimensional radiative transfer model. The need for such a model is further emphasized by planned satellite missions of tropical zone radiation and rainfall observations.[1]

Three-dimensional models of radiative transfer in raining clouds are limited. Passive microwave modeling of convective clouds and rainfall[7,8] considered three-dimensional cloud structures but only one-dimensional radiative transfer. Wilheit *et al.*[9] developed a one-dimensional radiative transfer model for determining microwave brightness temperatures as functions of rainfall rates. Kummerow and Wein-

J. L. Haferman, W. F. Krajewski, and T. F. Smith are with the University of Iowa, Iowa City, Iowa 52242. J. L. Haferman and T. F. Smith are with the Department of Mechanical Engineering; W. F. Krajewski is with the Department of Civil and Environmental Engineering, Iowa Institute of Hydraulic Research. A. Sánchez A. is with the Escuela de Ingeniería Mecánica, Universidad de los Andes, Merida, Venezuela.

Received 1 June 1992
0003-6935/93/152795-08$05.00/0.

man[4] and Weinman and Kummerow[10] presented simulations by using a two-layer, plane-parallel radiative transfer model for precipitating clouds.

The objective of this paper is to examine the microwave brightness temperature for a three-dimensional raining cloud. The atmospheric system considered, which is depicted in Fig. 1, consists of a cloud, a rain cell, a surface, and the atmosphere. The cloud is a finite layer with base and top heights of H_b and H_t, respectively, and length L_c for the x and z directions, and has the same structure as that given by Wilheit *et al.*[9] The rain has a footprint area of $L_r \times L_r$, a rainfall rate R, and extends from the bottom of the cloud to the surface. A single rain cell and cloud are considered. The surface is isothermal, opaque, and diffusely emitting and reflecting. The atmosphere is composed of radiatively participating water vapor and oxygen and other radiatively transparent gases. Specific values of the parameters are cited below. The microwave brightness temperature corresponds to the equivalent blackbody temperature of the upwelling radiant intensity at the cloud top $I(x, H_t, z, \bar{\omega}_d)$, where $\bar{\omega}_d$ denotes the direction of the sensor. The brightness temperature is sought as a function of the rain footprint area, rainfall rate, and cloud top height.

The governing equations are introduced in the next section. The solution methodology is then reviewed. Values for the parameters appearing in the formulation of the raining cloud systems are cited. Results and discussion are then presented.

Governing Equations

The continuous forms of the governing equations are presented to illustrate the types of equation being solved by the numerical model. The equations consist of the radiative transfer equation for the radiant intensity and the boundary conditions. Spatial and spectral variations of the radiant properties and energy terms are allowed.

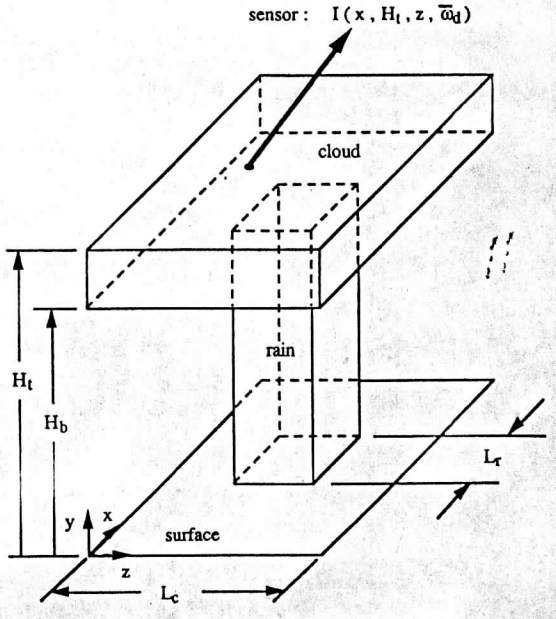

Fig. 1. Geometry for a raining cloud.

The propagation of radiation along a line-of-sight direction ζ is described by the radiative transfer equation. For unpolarized radiation, the change in the radiant intensity $I(\zeta)$ in the $\bar{\omega}$ direction is expressed by the radiative transport equation, which is stated by

$$\frac{dI}{d\zeta} = -\beta I(\zeta) + S(\zeta), \tag{1}$$

where the radiation source function is

$$S(\zeta) = aI_b + \frac{s}{4\pi}\int_0^{4\pi} I'(\zeta, \bar{\omega})\Phi(\omega', \bar{\omega})d\omega'. \tag{2}$$

The spatial and wavelength dependencies of all radiant energy and property quantities are understood. The primes denote an incoming quantity. In Eqs. (1) and (2), β is the extinction coefficient given by the sum of the absorption coefficient a and the scattering coefficient s, Φ is the scattering phase function for radiant energy that is incident within solid angle ω' about the $\bar{\omega}'$ direction and scattered into solid angle ω about the $\bar{\omega}$ direction. The scattering phase function is normalized such that

$$\frac{1}{4\pi}\int_0^{4\pi} \Phi(\bar{\omega}', \bar{\omega})d\omega = 1. \tag{3}$$

The boundary condition for the radiant intensity at the surface ($z = 0$) and for the $\bar{\omega}$ direction is expressed as

$$I^+ = \epsilon_0 I_b{}^+ + \frac{\rho_0}{\pi}\int_0^{2\pi} I^-(\bar{\omega}')\eta' d\omega'. \tag{4}$$

In Eq. (4), the superscripts + and − indicate radiation going from the boundary toward the medium inside the domain and from the medium toward the boundary. The surface has an emittance ϵ_0, a blackbody intensity $I_b{}^+$, which depends on the temperature of the surface, and a diffuse reflectance $\rho_0(=1-\epsilon_0)$. The cosine of the angle between the direction of propagation of I^- and the normal to the surface is η. All other boundaries are transparent to radiation and have no radiant energy sources.

Solution Methodology

In view of the complexities inherent in Eqs. (1)–(4), solutions for the radiant intensity are sought by using a numerical procedure. One such procedure that has a wide range of capabilities is the discrete-ordinates method. Several formulations of the discrete-ordinates method are available.[11–17] The present formulation has been extracted from Sánchez *et al.*[17] The discretized form of the radiative transport equation in Eq. (1) is obtained by subdividing the entire three-dimensional domain into cubical control

volumes and discretizing the direction of propagation of the radiant intensity. Typical control volumes are shown in Fig. 2, where control volume P with differential volume $\Delta V = \Delta x \Delta y \Delta z$ is of interest. Control volume P is surrounded by six adjacent control volumes labeled W (west), E (east), S (south), N (north), F (front), and B (back) with associated interfaces of w, e, s, n, f, and b. Each control volume is homogeneous, and nonhomogeneities are accounted for by assigning different radiative properties to the control volumes.

In terms of the reference intensities, the average intensity I_i^P for control volume P in discrete direction i is given by

$$I_i^P = \frac{\frac{\mu_i}{\Delta x} I_i^{xr} + \frac{\delta_i}{\Delta y} I_i^{yr} + \frac{\gamma_i}{\Delta z} I_i^{zr} + \alpha S}{\frac{\mu_i}{\Delta x} + \frac{\delta_i}{\Delta y} + \frac{\gamma_i}{\Delta z} + \alpha\beta}, \tag{5}$$

where the direction cosines μ_i, δ_i, and γ_i are for the x, y, and z directions, respectively. The superscript r designates the interface from which the radiant energy originates for the indicated coordinate. In Eq. (5), the finite difference weighting factor α is taken as unity.[17] The intensities arriving at the end faces (which become the reference intensities for the neighboring control volumes) are recovered from

$$I_i^{xe} = [I_i^P + (\alpha - 1) I_i^{xr}]/\alpha. \tag{6}$$

Expressions for y and z are written by interchanging x with y and z. The source term is composed of the emission and inward scattered intensities, and is expressed by

$$S = aI_b^P + \frac{s}{4\pi} \sum_{j=1}^{K} w_j I_j^P \Phi_{ij}, \tag{7}$$

where K represents the total number of discrete directions and w_j is the angular quadrature weight for direction j. The boundary condition from Eq. (4) becomes

$$I^+ = \epsilon_0 I_b^+ + \frac{\rho_0}{\pi} \sum_{\Omega_i < 0} I^- \Omega_i w_i. \tag{8}$$

With the radiative transfer equations discretized, a solution is obtained by solving for the radiant intensities, given the boundary conditions and radiative properties.

The quadrature set selected is the level sequential-odd quadrature. The discrete ordinates are referred to as S–N, where the total number of directions is $K = N(N + 2)$. Quadrature sets are generated from a computer code and agree with those listed by Fiveland.[18] Results presented below are produced by using $N = 6$.

For energy to be conserved, the quadrature set must accurately integrate the scattered intensities, that is, the terms of $w_j I_j \Phi_{ij}$ in Eq. (7), for all forms of the phase functions. Because the integration procedure has already been selected, the phase function may need modifying in order to guarantee conservation of energy. An accurate integration procedure results from expanding the phase function in a series of Legendre polynomials (P_n) as follows:

$$\Phi_{ij} = \sum_{n=0}^{M_1} (2n + 1) b_n P_n(\cos \theta_{ij}), \tag{9}$$

where M_1 represents the number of terms in the series and b_n are coefficients for the series expansion of the phase function in terms of the Legendre polynomials of order n. The cosine of the angle between discrete directions i and j is evaluated from

$$\cos \theta_{ij} = \mu_i \mu_j + \delta_i \delta_j + \gamma_i \gamma_j. \tag{10}$$

The representation of the phase function in terms of Legendre polynomials is advantageous in that it allows for the accurate evaluation of this function between any two directions based on known discrete values. When a quadrature set is used in the integration of Eq. (9), energy conservation may not be satisfied for values of N that yield reasonable computational times. To address this concern, the phase function is renormalized for every wavelength. The renormalized phase function $\bar{\Phi}_{ij}$ is obtained from

$$\bar{\Phi}_{ij} = \Phi_{ij} \Big/ \frac{1}{4\pi} \sum_{i=1}^{K} w_i \Phi_{ij}. \tag{11}$$

For the wavelengths of interest in the microwave region, the scattering phase function for the water

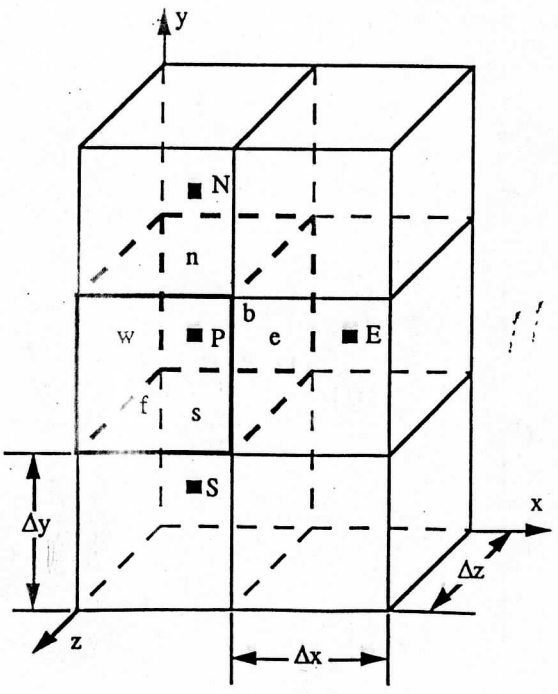

Fig. 2. Control volumes.

droplets is not highly anisotropic,[9] which thereby negates the need to apply the δ-M and scaling methods.[17]

The intensity directed toward the satellite in directions other than those of the discrete quadrature set may be found. The intensities from Eq. (5) contain enough information to describe the entire radiation field and to evaluate the source term S that is required for applying Eq. (5) to any sensor direction $(\mu_d, \delta_d, \gamma_d)$. The set of discrete intensities I_i^P are known throughout the entire domain. The intensities in the direction of the satellite are calculated by evaluating the boundary intensities from Eq. (8) and the source terms from Eq. (7), and then applying Eqs. (5) and (6) to obtain the desired output intensities. This procedure does not require interpolation of the intensities between the discrete directions.

The brightness temperature for intensity I and wavelength λ is evaluated from the Rayleigh–Jeans approximation:

$$T_b = I\frac{\lambda^4 C_2}{2C_1}, \tag{12}$$

where C_1 and C_2 are first and second constants in the Planck spectral blackbody distribution, respectively.

Parameters

Values of several model parameters for the atmospheric system shown in Fig. 1 are presented in Table 1. The cloud thickness $(H_t - H_b)$ remains a constant at 0.5 km.[9] Also, the radiant energy is viewed at a frequency of 19.355 GHz. The temperature profile in the atmosphere is given by

$$T(y) = \alpha_t(y - H_t) + T_t, \tag{13}$$

where α_t is the temperature gradient in the atmosphere (−6.5 K/km) and the temperature at the cloud top T_t is taken as the freezing point of water (273.17 K). Because the atmospheric temperature varies with y, all radiative properties depend on y. The relative humidity ϕ is the ratio of the mass of water vapor in the air to the mass of water vapor in saturated air at a given temperature and is assumed to vary linearly with elevation from the surface value of $\phi_0 = 80\%$ to the cloud top value of $\phi_t = 100\%$. Modeling air and water vapor as ideal gases, we determine the partial pressure of water vapor from

$$P_v = \phi P_s(T), \tag{14}$$

where P_s is the saturation pressure of water vapor at temperature T. The expression for P_s as a function of temperature is given by the American Society of Heating, Refrigerating and Air-Conditioning Engineers.[19]

The raindrop size distribution for the number density of particles per unit size interval is formulated by using the Marshall–Palmer distribution[9]:

$$N(r) = N_0 \exp(-\Lambda r), \tag{15}$$

where N_0 is a proportionality constant, Λ is the exponential parameter, and r is the radius of a drop. In terms of the rainfall rate R (in millimeters per hour), the exponential parameter is given by

$$\Lambda = 81.56R^{-0.21}. \tag{16}$$

To use Eq. (16) in Eq. (15), r must have units of centimeters. For this study, the raindrop size distribution is scaled with air density[9] so that the scaled Marshall–Palmer distribution becomes

$$\tilde{N}(r) = \left[\frac{D_a(0)}{D_a(y)}\right]^{-0.4} N(r). \tag{17}$$

The variation of the local air density D_a with y is taken from Ulaby *et al.*[20]

Absorption and scattering are linear processes. For the atmospheric system under consideration, the mixture radiative coefficients at altitude y are given by[20]

$$\gamma(y) = \gamma_g(y) + \gamma_c(y) + \gamma_r(y), \tag{18}$$

where the generalized radiative coefficient γ represents a, s, or β, and subscripts g, c, and r refer to gases, clouds, and rain, respectively. For atmospheric gases, only absorption is considered, and the absorption coefficient is

$$a_g(y) = a_{H_2O}(y) + a_{O_2}(y), \tag{19}$$

where H_2O and O_2 refer to water vapor and oxygen, respectively. Expressions for the absorption coefficients of water vapor and oxygen as functions of atmospheric pressure, temperature, and water vapor density are given by Ulaby *et al.*[20] and are not presented here. The atmospheric pressure at altitude y is calculated from the ideal gas relation by using the local air density, the gas constant for air,

Table 1. Model Parameters

Radiative transfer	f, 19.355 GHz λ, 1.55 cm θ, 0 deg
Freezing level	H_t, 1–5 km T_t, 273.1 K ϕ_t, 100%
Cloud	D_c, 0.5 g/m^3 $H_t - H_b$, 0.5 km L_c, 19 km
Raindrops	N_0, 0.16 cm^{-4} r_{min}, 0.0054 cm r_{max}, ∞ R, 0–300 mm/h
Ocean surface	ϕ_0, 80% ρ_0, 0.6 ϵ_0, 0.4

and the local temperature from Eq. (13). The water-vapor density is determined from the ideal gas equation of state by using the partial pressure of water vapor from Eq. (14), the gas constant for water vapor, and the temperature from Eq. (13). The radiative coefficients for rain are computed from

$$\gamma_r(y) = \int_{r_{min}}^{r_{max}} Q_r \pi r^2 \tilde{N}(r) dr, \tag{20}$$

where values for r_{min} and r_{max} are cited in Table 1, and Q_r is the absorption, scattering, or extinction efficiency factor for a spherical liquid-water droplet.[21] The efficiency factors are functions of the radius of the droplet and the complex refractive index of liquid water. Data for the complex refractive index of liquid water are extracted from Lane and Saxton[22] and are functions of wavelength and local temperature.

The cloud water droplet sizes are taken to be much smaller than the wavelength of incident radiation, and, thus, the Rayleigh approximation is valid.[20] For water spheres in the Rayleigh region, scattering is negligible. The cloud absorption coefficient is evaluated from

$$a_c = a_1 D_c, \tag{21}$$

where the coefficient a_1 is evaluated from

$$a_1 = \frac{6\pi}{\lambda} \mathrm{Im}\left(\frac{n^2 - 1}{n^2 + 2}\right), \tag{22}$$

and D_c is the cloud liquid-water content (Table 1). In Eq. (22), the wavelength λ is in micrometers and the complex refractive index n of liquid water is a function of wavelength and local temperature.[22]

Results and Discussion

The three-dimensional raining atmosphere model and its numerical implementation were validated by using several one-, two-, and three-dimensional examples, as discussed by Sánchez *et al.*[17,23] These examples demonstrated that the model is capable of reproducing results from existing studies. The first set of results considers one-dimensional radiation only. Subsequent results examine the effects of three-dimensional radiation and compare the one-dimensional results with three-dimensional results at the same x–z location and the same atmospheric composition in the vertical structure. Finally, results are presented to examine the effects of the viewing position for three-dimensional radiation.

The first numerical experiment considers the effect of cloud height and rainfall rate on upwelling brightness temperatures detected by the satellite sensor viewing the cloud top. This experiment is designed after Wilheit *et al.*[9] and serves to validate the three-dimensional model for a plane layer. The three-dimensional discrete-ordinates method is used to solve for brightness temperatures in a one-dimensional system by using the short-cut method developed by Sánchez *et al.*[23]

Results are presented in Fig. 3 for plane-layer brightness temperatures sensed at the cloud top, with the satellite sensor positioned at nadir. The results show that, for a given rain rate, brightness temperatures increase with increasing cloud top height. This trend occurs because the cloud top temperature is assumed to be fixed, as is the temperature gradient. As the cloud top height increases, the ocean surface temperature also increases. The satellite sensor sees a warmer atmosphere and ocean as the cloud top height rises. For a fixed cloud top height, brightness temperatures increase with increasing rain rates, reach a maximum, and then decrease beyond some critical rain rate. As the rain rate increases, the satellite sensor sees the warmer, strongly emitting raindrops. For higher rain rates, the brightness temperatures for all the cloud top height conditions decrease and reach a saturation point. The saturation point is due to the layers becoming optically thick, and the sensor then sees only the topmost raining layer. The decrease in brightness temperature is due to stronger backscattering at higher rain rates. These results compare favorably with those presented by Wilheit *et al.*[9]

Results examining dimensionality effects are shown in Fig. 4. For these results, the satellite sensor is placed at the top and center of a 19 km × 5 km × 19 km atmospheric system, with a 1 km × 1 km rain field centered beneath the cloud. The cloud top is 5 km above the ocean surface. For no rain, the brightness temperature for the one-dimensional model is 197 K. The results from Fig. 4 show that the brightness temperatures calculated for the three-dimensional case are, in general, significantly lower than the corresponding brightness temperatures generated from the one-dimensional model.

The difference in brightness temperatures depicted in Fig. 4 is perhaps better realized from an examination of Fig. 5, which shows the difference between the one- and the three-dimensional brightness temperatures for the parameters cited in Table 1. The

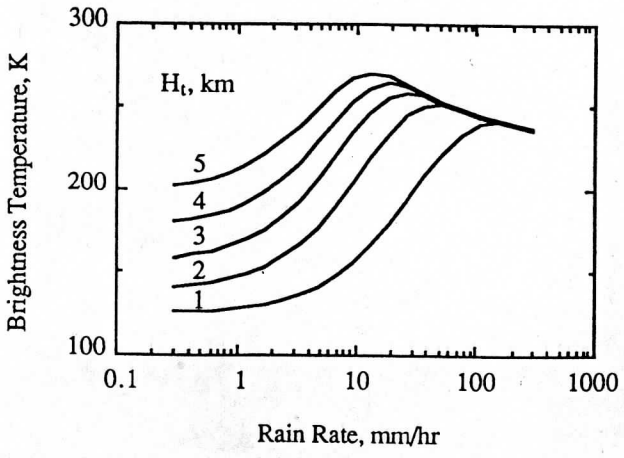

Fig. 3. Three-dimensional model validation of plane layer (20 layers).

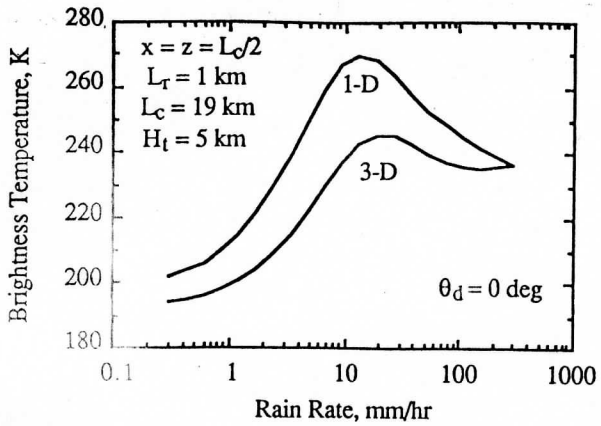

Fig. 4. Dimensionality effects: three-dimensional versus one-dimensional.

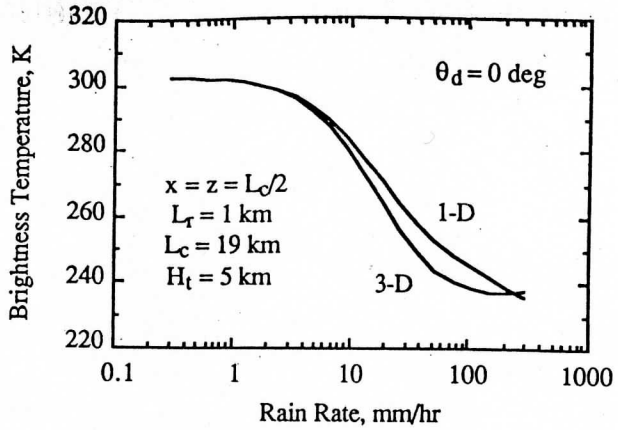

Fig. 6. Surface reflectance effect ($\epsilon_0 = 1.0$).

results show that, for rain rates between approximately 1 and 100 mm/h, the difference in brightness temperature is more than 10 K, which is deemed significant. At higher rain rates, three-dimensional effects become less important as the raining layers become optically thick.

The results shown in Figs. 4 and 5 indicate that three-dimensional effects are apparent even at low rain rates. For example, for R = 0.3 mm/h, the difference in brightness temperature between the one- and the three-dimensional results is ~8 K. These results are surprising because, at low rain rates, the scattering contribution from the raindrops is negligible, and there is no scattering contribution from the atmosphere itself. An explanation is given by considering that, in the three-dimensional model, the ocean reflects a portion of incident radiation. Therefore, for the three-dimensional radiation results, the contribution to radiation from a volume of atmosphere outside the rain area and reflected by the surface underneath the rain area in the direction of the sensor is small, thereby yielding a lower brightness temperature.

To verify the effect of the surface reflectance, the previous experiment was repeated with the ocean modeled as a nonreflecting surface. The results are shown in Fig. 6 for the one- and the three-dimensional models. The brightness temperatures decrease as the rain rate increases. For no rain, the brightness temperature is 303 K. At low rain rates, the one- and the three-dimensional results are in agreement because, in the absence of scattering by the rain and reflection from the surface, the satellite receives radiation from a column of atmosphere. At higher rain rates, the three-dimensional brightness temperatures are lower than the one-dimensional temperatures because of scattering in off-sensor directions. At high rain rates, three-dimensional effects become small because of increasing optical thickness of the rain cell.

The effects of the rainfield footprint length L_r on the brightness temperature are shown in Fig. 7, with the sensor looking at the radiant intensity at $x = z = L_c/2$. As the rainfield approaches the size of the solution domain, the three-dimensional results approach the one-dimensional results. For example, when L_r = 19 km, the brightness temperature at the center of the cloud for the three-dimensional model is 264.4 K, which is nearly equal to that for the one-dimensional model (267.4 K). The neglect of radiant

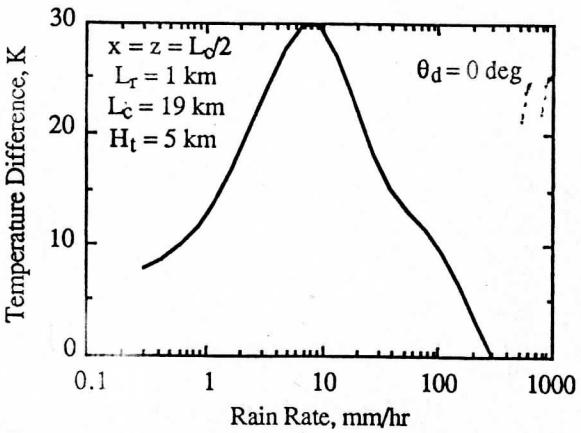

Fig. 5. Dimensionality effects: brightness temperature difference.

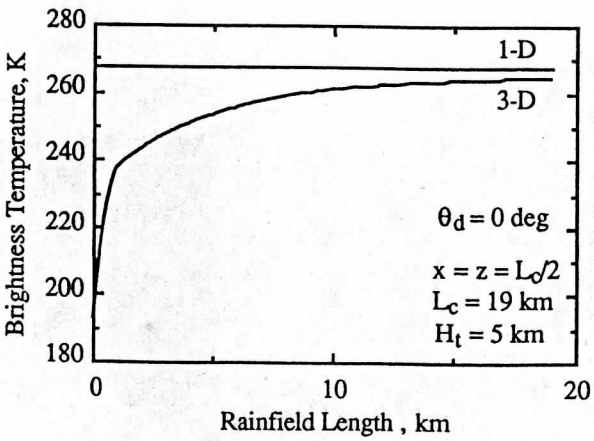

Fig. 7. Effect of rain footprint.

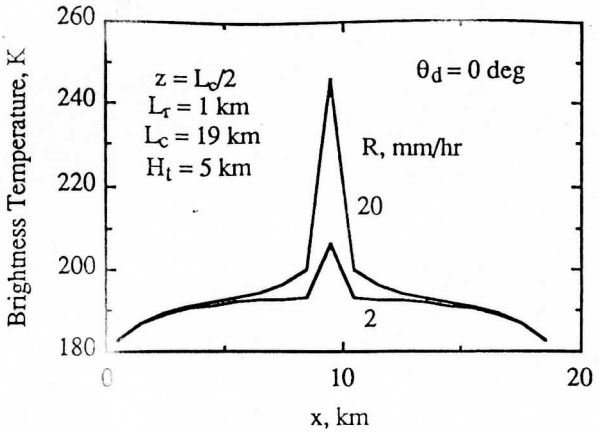

Fig. 8. Viewing position effects.

energy from the atmosphere outside the solution domain accounts for this difference.

The last numerical experiment examines the effects of the satellite viewing position on three-dimensional brightness temperature calculations. Brightness temperatures are illustrated in Fig. 8 for satellite scans along the top of the cloud at $z = L_c/2$ and for the nadir viewing angle. Results are shown for rain rates of $R = 2$ and 20 mm/h. For comparison, the brightness temperatures for a one-dimensional atmospheric system are 198 K with no cloud and no rain, 197 K with a cloud but no rain, and 223 K for $R = 2$ mm/h. As shown in Fig. 8, a rapid increase in brightness temperature occurs as the satellite passes over the rainfield. Unless the satellite is directly over the rainfield, the rain has a small effect on the brightness temperatures seen by the satellite. For the higher rain rate, an increase in brightness temperature is noticed approximately 5 km from the rainfield. The brightness temperature decrease near the cloud edge is due to neglecting radiant energy from the atmosphere outside the solution domain that is reflected by the surface. Near $x = 5$ km, the brightness temperature is 191 K, which is 6 K lower than that for a one-dimensional atmosphere with no rain. Again, neglecting radiant energy from the atmosphere that is outside the solution domain and reflected by the surface into the direction of the satellite yields a lower brightness temperature at this location.

Conclusions

Microwave brightness temperatures for a three-dimensional raining cloud over a reflecting surface have been computed by using a radiative transfer model based on the discrete-ordinates method. Comparisons of brightness temperatures from the three-dimensional model for a plane layer with those available in the literature for a one-dimensional model validate the model. Other results illustrate three-dimensional effects of upwelling brightness temperatures by considering rainfall rate, cloud top height, and satellite sensor viewing position. The results indicate that, under certain circumstances, three-dimensional effects are significant, and the influence of the surface reflectance may be important.

Recommendations for future work include an ongoing analysis of three-dimensional radiation effects on satellite-sensor-based rainfall retrieval algorithms. It is anticipated that three-dimensional effects may become even more pronounced at higher frequencies and for atmospheric conditions in which ice is present.[4,5,8,10] The results in this paper show that the surface reflectance is an important parameter for determining three-dimensional effects. In view of this finding, the bidirectional reflectance for the surface may play a more important role than that found in previous studies.[24] A more accurate representation of cloud fields, perhaps using fractals,[25] should be explored. Incorporation of a spatial integration procedure to account for satellite footprint viewing effects and directions is desirable. An uncertainty analysis should be developed so that the degree of reliability of any rainfall retrieval algorithm can be estimated. Finally, a verification of the three-dimensional results with actual experimental results should be performed.

The authors acknowledge partial support for this study from grant NA89AA-D-AC195, National Oceanic and Atmospheric Administration: Global Change Program. J. Haferman was partially supported by a Graduate Fellowship provided by the NASA Iowa Space Grant Consortium. A. Sánchez A. recognizes the financial support received from Universidad de los Andes and Fundación Gran Mariscal de Ayacucho, both of the Republic of Venezuela. Portions of this work were performed with the supercomputer facilities at the San Diego Supercomputer Center.

References

1. J. Simpson, R. F. Adler, and G. North, "A proposed tropical rainfall measuring mission (TRMM) satellite," Bull. Am. Meteorol. Soc. **69,** 278–295 (1988).
2. P. Arkin and P. Ardanuy, "Estimation of climatological scale precipitation from space: a review," J. Climate **2,** 1229–1238 (1989).
3. J. C. Alishouse, R. R. Ferraro, and J. V. Fiore, "Inference of oceanic rainfall properties from the Nimbus 7 SMMR," J. Appl. Meteorol. **29,** 551–560 (1990).
4. C. D. Kummerow and J. A. Weinman, "Determining microwave brightness temperatures from precipitating horizontal finite and vertically structured clouds," J. Geophys. Res. **93,** 3720–3728 (1988).
5. T. T. Wilheit, A. T. C. Chang, J. L. King, E. B. Rodgers, R. A. Nieman, B. M. Krupp, A. S. Milman, J. S. Stratigos, and H. Siddalingaiah, "Microwave radiometric observations near 19.35, 92 and 183 GHz of precipitation in tropical storm Cora," J. Appl. Meteorol. **21,** 1137–1145 (1982).
6. T. T. Wilheit, A. T. C. Chang, and L. S. Chiu, "Retrieval of monthly rainfall indices from microwave radiometric measurements using probability distribution functions," J. Atmos. Ocean. Technol. **8,** 118–136 (1991).
7. A. Mugnai, H. J. Cooper, E. A. Smith, and G. J. Tripoli, "Simulation of microwave brightness temperatures of an evolving hailstorm at SSM/I frequencies," Bull. Am. Meteorol. Soc. **71,** 2–13 (1990).
8. R. F. Adler, H-Y. M. Yeh, N. Prasad, W-K. Tao, and J. Simpson,

"Microwave simulations of a tropical rainfall system with a three-dimensional cloud model," J. Appl. Meteorol. **30,** 924–953 (1991).
9. T. T. Wilheit, A. T. C. Chang, M. S. B. Rao, and J. S. Theon, "A satellite technique for quantitatively mapping rainfall rates over the oceans," J. Appl. Meteorol. **16,** 551–560 (1977).
10. J. A. Weinman and C. D. Kummerow, "A radiative transfer model of microwave radiances from horizontally finite clouds containing ice and liquid hydrometeor layers," in *Tropical Rainfall Measurements,* J. S. Theon and N. Fugono, eds. (Deepack, Hampton, Va., 1988), pp. 325–336.
11. B. G. Carlson and K. D. Lathrop, "Transport theory, the method of discrete-ordinates," in *Computing Methods in Reactor Physics,* H. Greenspan, C. N. Kelber, and D. Okrent, eds. (Gordon & Breach, New York, 1968), pp. 171–266.
12. S. A. W. Gerstl and A. Zardecki, "Discrete-ordinates finite-element method for atmospheric radiative transfer and remote sensing," Appl. Opt. **24,** 81–93 (1985).
13. K. Stamnes, S-C. Tsay, W. Wiscombe, and K. Jayaweera, "Numerically stable algorithm for discrete-ordinate-method radiative transfer in multiple scattering and emitting layered media," Appl. Opt. **27,** 2502–2509 (1988).
14. W. A. Fiveland, "Three-dimensional radiative heat transfer solutions by the discrete-ordinates method," J. Thermophys. Heat Transfer **2,** 309–316 (1988).
15. W. A. Fiveland and A. S. Jamaluddin, "Three-dimensional spectral heat transfer solutions by the discrete-ordinates method," in *Heat Transfer Phenomena in Radiation, Combustion, and Fires,* R. K. Shah, ed. (American Society of Mechanical Engineers, New York, 1989), Vol. 106, pp. 43–48.
16. T. K. Kim and H. S. Lee, "Radiative transfer in two-dimensional anisotropic scattering media with collimated incidence," J. Quant. Spectrosc. Radiat. Transfer **42,** 225–238 (1989).
17. A. Sánchez, W. F. Krajewski, and T. F. Smith, *A General Purpose Radiative Transfer Model for Application to Remote Sensing in Multi-Dimensional Systems,* IIHR Rep. 355 (Iowa Institute of Hydraulic Research, The University of Iowa, Iowa City, Iowa, 1992).
18. W. A. Fiveland, "The selection of discrete ordinate quadrature sets for anisotropic scattering," in *Fundamentals of Radiation Heat Transfer,* W. A. Fiveland, A. L. Crosbie, A. M. Smith, and T. F. Smith, eds. (American Society of Mechanical Engineers, New York, 1991), Vol. 160, pp. 89–96.
19. *1985 ASHRAE Handbook—Fundamentals* (American Society of Heating, Refrigerating and Air-Conditioning Engineers, Atlanta, Ga., 1985).
20. F. T. Ulaby, R. K. Moore, and A. K. Fung, *Microwave Remote Sensing Fundamentals and Radiometry* (Artech, Norwood, Mass., 1981), Vol. I.
21. C. F. Bohren and D. R. Huffman, *Absorption and Scattering of Light by Small Particles* (Wiley, New York, 1983).
22. J. A. Lane and J. A. Saxton, "Dielectric dispersion in pure polar liquids at very high radio frequencies," Proc. R. Soc. London Ser. A **213,** 400–408 (1952).
23. A. Sánchez, T. F. Smith, and W. F. Krajewski, "Dimensionality issues in modeling with the discrete-ordinates method," submitted to J. Heat Transfer.
24. H. W. Barker and J. A. Davies, "Solar radiative fluxes for broken cloud fields above reflecting surfaces," J. Atmos. Sci. **49,** 749–761 (1992).
25. A. Davis, P. Gabriel, S. Lovejoy, D. Schertzer, and G. L. Austin, "Discrete angle radiative transfer 3. Numerical results and meteorological applications," J. Geophys. Res. **95,** 11,729–11,742 (1990).